Article type: Feature Article

Dimensional confinement in carbon-based structures – From 3D to 1D

Nils Richter[1,2], Zongping Chen[3], Marie-Luise Braatz[1,2], Fabienne Musseau[1], Nils-Eike Weber[4,#], Akimitsu Narita[3], Klaus Müllen[3,5,], Mathias Kläui[1,2,*]*

*Corresponding Author: E-mail: klaeui@uni-mainz.de; muellen@mpip-mainz.mpg.de

[1]Johannes Gutenberg Universität, Institut für Physik, Staudingerweg 7, 55128 Mainz, Germany
[2]Graduate School Materials Science in Mainz, Staudingerweg 9, 55128 Mainz, Germany
[3]Max Planck Institut für Polymerforschung, Ackermannweg 10, 55128 Mainz, Germany
[4]Carbon Materials Innovation Center (CMIC), BASF SE, Carl-Bosch-Straße 38, 67056 Ludwigshafen, Germany
[5]Johannes Gutenberg Universität, Institut für physikalische Chemie, Duesbergweg 10-14, 55128 Mainz, Germany
[#]Current address: Scienta Omicron GmbH, Limburger Str. 75, 65232 Taunusstein, Germany

Abstract

We present an overview of charge transport in selected one-, two- and three-dimensional carbon-based materials with exciting properties. The systems are atomically defined bottom-up synthesized graphene nanoribbons, doped graphene and turbostratic graphene micro-disks, where up to 100 graphene layers are rotationally stacked. For turbostratic graphene we show how this system lends itself to spintronic applications. This follows from the inner graphene layers where charge carriers are protected and thus highly mobile. Doped graphene and graphene nanoribbons offer the possibility to tailor the electronic properties of graphene either by introducing heteroatoms or by confining the system geometrically. Herein, we describe the most recent developments of charge transports in these carbon systems.

1. Introduction

Carbon-based materials offer a large number of advantageous properties, and hence have attracted a great deal of attention in science and in industry, with applications ranging from micro-electronics to energy related topics [1,2]. As carbon can come in very different forms of allotropes having distinct structures and attributes, the possibilities for its use may well be exceeding those of other elements. Sp^2-hybridized carbon materials alone i.e. graphite,

graphene, carbon nanotubes, graphene nanoribbons or fullerenes can exhibit unique qualities, such as high mechanical strength and excellent electrical, thermal and spin transport properties [3–7]. Often, there is a close relationship between such features and the crystalline structure. Thus, by tailoring the structure and dimensionality, one has the chance to modulate the properties of the system. In three dimensions, one prominent example is graphite. Despite the fact that graphene is the building block of graphite, the Bernal stacking of layers causes a drastic change in the electronic band structure [8,9] as compared to the two-dimensional single layer of graphene. However, turbostratic and epitaxial graphene exhibit a rotated layered arrangement, which can electronically decouple the layers in an energy-interval around the K-point [10,11]. Indeed, electrons in epitaxial multilayer graphene, grown on silicon carbide have a linear energy dispersion near the Dirac point, due to the rotation of the layers with respect to each other [12]. Turbostratic graphene disks exhibit furthermore a special quality: a particularly high charge carrier mobility of up to $10^4\ \mathrm{cm^2/Vs}$ in its central layers which are protected from the environment [13].

Graphene was the first in the family of “2D-materials” to appear in the spotlight after having been experimentally studied in-depth for the first time in 2004 [14,15]. Realizing the vast potential of this group of materials, other mono- and few-layer systems like MoS_2 [16] and black phosphorus [17] are becoming the subject of extensive research. The promises to use 2D-materials and especially graphene in technological applications are a strong driving force here. To date many different approaches have been developed to obtain graphene, such as mechanical exfoliation, epitaxial growth and liquid-phase exfoliation through intercalation [18]. Growing graphene with chemical vapor deposition (CVD) offers advantages compared to other methods concerning the scalability of this process, which allows for the production of large homogeneous films. However, while especially mechanical exfoliation can yield very high quality graphene, which manifests itself, for example, in a high charge carrier mobility, CVD-

graphene has previously lagged behind in this aspect. Only recently, mobilities of up to $350\,000\ \mathrm{cm^2/Vs}$ have been measured after the optimization of the growth and the transfer processes [19].

While in its pure form graphene is inherently a two-dimensional material, graphene nanoribbons (GNRs) and carbon nanotubes (CNTs) are significantly confined along one lateral dimension and thus become (quasi-)one-dimensional [20,21]. The geometrical confinement has a strong effect on the electronic properties of GNRs and CNTs. In fact, if the translational symmetry of the crystal lattice is broken, a band gap opens up [22,23]. In CNTs, the gap depends on the chirality of the tube, i.e. how much the crystal direction of the hexagonal lattice is twisted along the longitudinal axis of the tube [24]. Certain factors such as the size and morphology of nucleation centers determine the chirality of a CNT during its growth process [25]. Yet, a fully chirality-selective synthesis has not been achieved [26]. In contrast, in GNRs, where the band gap is defined by the crystal direction, the edge structure and the width of the ribbon, the synthetic method has been advancing significantly over the recent years. Through a bottom-up chemical approach GNRs can be synthesized with structural perfection on the atomic level [20,27,28].

In this paper, we concisely summarize our recent research activities on three selected carbon materials: turbostratic graphene disks, N-doped graphene films and chemically synthesized GNRs, in particular, focusing on their electronic structure. Each of these is a representative of a three-dimensional, two-dimensional and one-dimensional world respectively and exhibits characteristic charge transport properties.

2. 3D: Turbostratic graphene disks

Turbostratic graphene (TG) is a stack of graphene where every adjacent layer is rotated by a certain angle, which leads to a restoration of the linear band structure in an energy window around the K-point known from single layer graphene [11]. Thus, in contrast to graphite, TG retains 2D-charge transport properties with high charge carrier mobilities in the order of $10^4\ \mathrm{cm^2/Vs}$ [13]. Due to its particularly low resistivity, the conductance mismatch problem for spin-injection in semiconductors [29] can be mitigated. As for graphene-based materials in general, there is a great potential to apply TG in spintronics, since graphene exhibits a low spin orbit coupling and weak hyperfine interaction [30,31]. In 2007, the first successful spin injection into graphene was demonstrated [7]. The high spin diffusion length, up to 30 μm [6], could be a key advantage of this material. To perform spin injection in single layer graphene a tunneling barrier is typically required in order to overcome the conductivity mismatch problem, which leads to the difficulty of growing a uniform oxide layer on graphene. We demonstrate efficient spin injection into multilayer graphene with a non-local resistance value up to 0.5 mΩ (**Figure 1**) [32], rendering it a highly promising material for spintronic applications such as in spin torque devices which have been demonstrated only in metal-based systems up to date [33,34].

2.1. Fabrication of TG disks

The TG disks are here fabricated by the decomposition of hydrocarbons by exposing them to the heat of an inert gas plasma, which can be carried out on an industrial scale in a plasma-arc reactor. This process leads to the generation of micro-domain graphitic materials, such as fullerenes, CNTs, open conical carbon structures (also called micro-cones) and preferentially flat TG micro-disks [35]. The TG disks can be separated from this mixture of materials by means of sonication, centrifugation and filtration [13].

2.2. Transport properties of TG disks

In order to obtain a higher spin injection into a graphene-based spin conduit, it is advantageous to use novel materials as injector electrodes. Heusler alloys, owing to their half-metallicity, are predicted to have 100% spin polarization at the Fermi energy. Recently, Yamaguchi *et al.* demonstrated the efficient combination of a graphene-based spin valve and a Heusler compound as the injector [36]. A non-local signal of 430 Ω, which is the largest value for graphene-based devices so far, was reported.

In order to make optimal use of the spin transport properties of TG for the manipulation of local magnetization patterns in a ferromagnet, we modify the device architecture as follows. Unlike standard non-local spin valves where stripe-like ferromagnetic electrodes are usually patterned, we tailor the injector and detector electrode into a half ring shape. This allows to accurately nucleate a domain wall under a precise angle, which can be displaced by a pure diffusive spin current provided by a non-magnetic spin conduit [33]. Domain walls have a homogeneous magnetization on both sides of the magnetic structure and this feature can be used in order to control the direction of the pure spin current injected in the non-magnetic material.

The anisotropic magnetoresistance effect (AMR) can be used to detect the presence of a domain wall in the area probed by a local 4-point measurement. By applying fields along different directions and relaxing the fields, domain walls can be spatially localized. According to **Figure 2**, a domain wall can be positioned in the contact area for angles between -10° and 30°. On the opposite, the magnetic structure will be outside the contact area for angles greater than 30° where the measured resistance is higher. This so-called mode étoile measurement [37] is crucial in order to precisely probe the position of the domain wall and to control the direction of the incoming pure spin current that will act on the magnetization of the detector electrode [33].

Furthermore, we detect the non-local spin signal even without tunnel barriers, which usually help to overcome the conductivity mismatch for single layer graphene [7]. Hence, we conclude

that successful spin injection into TG and spin transport over micrometer distances is possible demonstrating that this material is a good candidate for use as a low-loss non-magnetic spin conduit. The transparent contacts allow for much higher current densities compared to tunnel contacts. Therefore, they will pave the way to achieve pure spin current injection through a multilayer graphene spin conduit leading to efficient spin-torques acting on a domain wall to displace it.

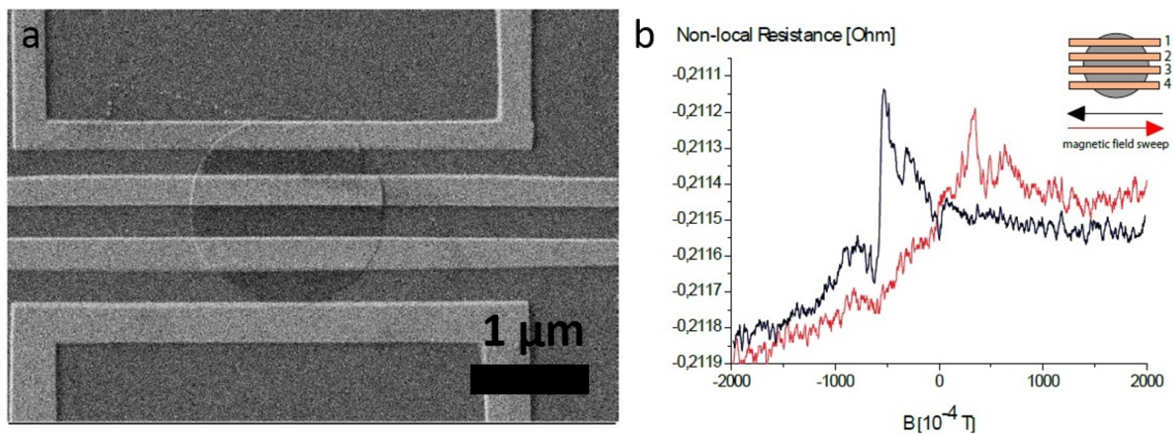

Figure 1: a) Scanning electron microscope (SEM) image of a non-local spin valve device, where cobalt electrodes were deposited on top of the TG disk. b) Non-local resistance measurement (current applied between electrodes 1 and 2 and spin current detected between electrodes 3 and 4). Images adapted from reference [32].

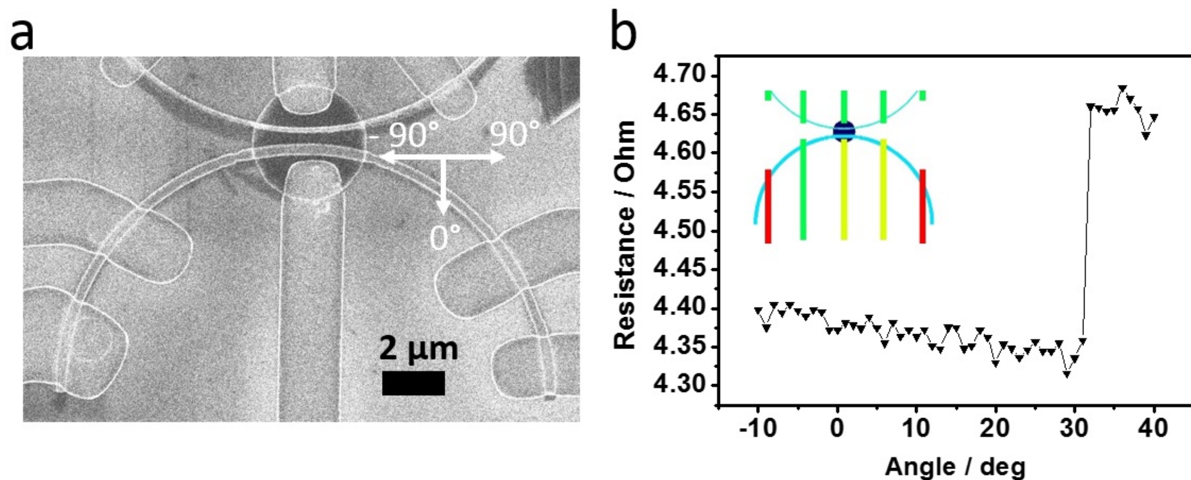

Figure 2: a) SEM image of a non-local spin valve device, where permalloy half rings and electrical contacts were deposited on top of the TG disk. b) Mode étoile measurement of the wide bottom injector electrode. Inset: Red marks the contacts for current injection and yellow the contacts for the voltage measurement.

3. 2D: Doped and undoped graphene

Unlike TG, where the multilayer structure allows to retain important properties of pure graphene due to the protection of central layers from environmental influence, a single layer of graphene is often doped by adatoms or charge puddles related to the supporting substrate [38–40]. In contrast to such uncontrolled alterations of graphene's electronic properties, a promising approach to tailor the band structure and the charge carrier properties is doping by heteroatoms, which are either incorporated in the lattice replacing carbon atoms [41], or physisorbed to the graphene surface while leaving the lattice intact [42,43]. Combining both approaches, allows for flexible transitions between n- and p-type doping in the same crystal, which demonstrates the versatility of changing the electronic properties in graphene by controlling the degree of doping [44]. Furthermore, heteroatomic doping has even the potential to open up a band gap [45–47]. Dopant concentrations of more than 15% have already been reached experimentally with nitrogen and boron [48–51]. However, while the band gap increased in the boron doped graphene, the mobility decreased due to a higher amount of backscattering effects [49]. This result indicates that the requirements for any device have to be carefully weighed against each other [48]. Improvements regarding one of the material's properties might lead to an undesired change of another one. The priorities have to be set according to the particular needs of the application in question.

3.1. Fabrication of doped graphene

Different fabrication methods can be used to incorporate the dopants into the graphene lattice. Hyperthermal ion implantation is an example for first growing pristine graphene and afterwards inserting the dopants [52]. Here the quality of the obtained doped graphene depends critically on the implantation beam energy and dose. Growing doped graphene in one step is also possible for instance by using CVD. For example, doping with nitrogen [51,53,54], boron [55,56], sulfur [57–59], phosphorus [60] and silicon [61] atoms has thus far been demonstrated by CVD.

Among them, nitrogen is often a natural choice as a dopant due to its comparable size to carbon while it hosts an additional valence electron. Furthermore, it can be easily integrated by using additional precursors like NH_3 or pyrrole [62]. To minimize lattice defects (such as vacancies) the growth parameters have to be carefully adjusted, which already enabled charge carrier mobilities of up to $350\ 000\ \mathrm{cm^2/Vs}$ in undoped graphene [19].

3.2. Magneto-transport properties and their relation to gradual structural modification

The nature of doping in graphene can be elucidated by investigating and comparing electrical transport and structural properties. Using Raman spectroscopy, it is possible to see phononic excitations and to obtain structural information [63]. In transport measurements we have probed the electrical resistance as a function of a perpendicularly applied magnetic field. In **Figure 3** we compare the Raman spectra and the magnetoresistance (MR) curves of several samples with different doping levels. The undoped graphene exhibits a small defect peak (D-peak) in the Raman spectrum, which is an indication for a small level disorder and doping. The intermediately doped samples have a higher D-peak and for the strongly doped sample the D-peak even tops both the G- and the 2D-peak. The magnetoresistance (MR) for these four samples also shows a strong dependence on doping as can be seen in **Figure 3** e)-f). The positive sign for the undoped curve can be described by the Lorentz-magnetoresistance while the negative MR of the strongly doped sample cannot be described by a single model.

The magnetoresistance exhibits a smooth transition from positive values for undoped graphene to negative values for strongly doped graphene [64]. Simultaneously varying a backgate-voltage and the magnetic field leads to a shift in the absolute values of the resistance as well as an altered relative behavior. The MR effect becomes the most pronounced near the Dirac point.

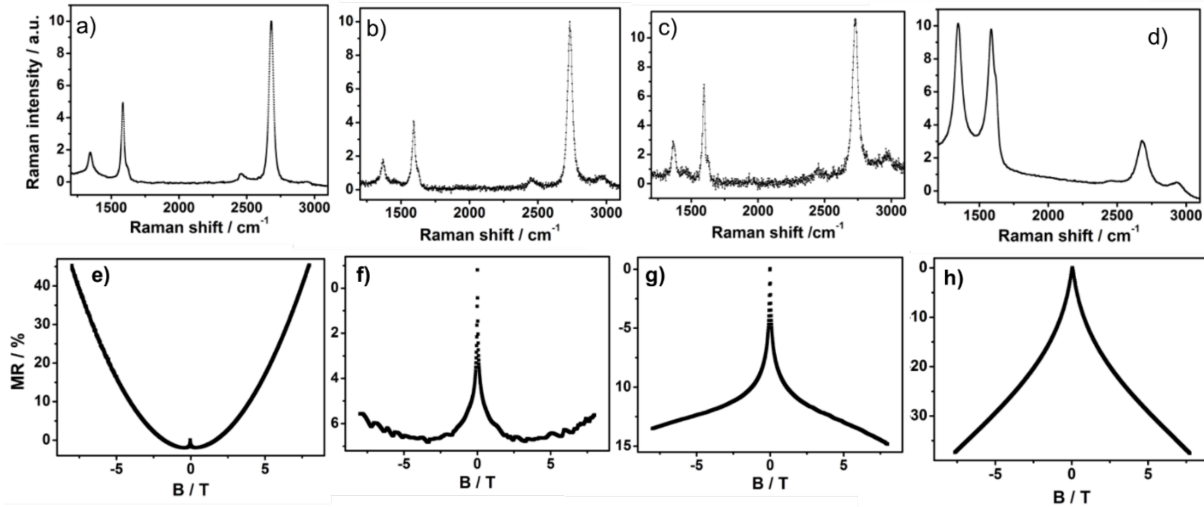

Figure 3: Raman spectra for a) undoped, b), c) lightly doped and d) strongly doped graphene. e)-f) show the MR effect for the same samples at temperatures between 2 and 3 K. a), d), e) and f) adapted with permission from Ref. [64]. Copyright 2015 American Chemical Society.

Looking at the temperature dependence of the resistance of these samples, a transport gap can be estimated by assuming Mott's 2D-variable range hopping model. For the strongly doped sample this leads to an activation energy or transport gap of (9.11 ± 0.55) meV [64] while for lower doping this goes down to (1.73 ± 0.28) meV for undoped graphene indicating some residual unintentional doping. However, for technological applications a transport gap due to localization effects is not sufficient because only a conventional semiconducting energy band gap allows for sizeable resistance modulations, as for example required in a field effect transistor. Transport gaps and band gaps can be discriminated by examining the temperature dependence of both resistivity and mobility at the same time [65]. Hence, simply increasing the doping to increase the band gap is not a straightforward route towards applications since this means, among other consequences, a reduction in charge carrier mobility.

Finally, weak localization (WL) can be seen as a peak in the MR-curves around 0 T (visible in all MR-curves **Figure 3** e)-f)) [30,66]. This effect can be observed in graphene at low temperatures and usually at small magnetic fields. It arises from backscattering and constructive interference between scattering paths that are identical and self-intersecting. WL leads to a rise

in resistance and is enhanced for doped graphene due to the additional scattering possibilities. It has been reported that WL is preserved up to room temperature in rather defective graphene with mobilities as low as $430\ \mathrm{cm^2/Vs}$ which was explained by the competition between valley-dependent scattering and the thermal dephasing due to the defects [67]. The opposite effect, weak anti-localization (WAL) occurs if the scattering paths are intersecting destructively, which leads to a decrease in resistance. Transitions between WL and WAL have been observed above a critical magnetic field [68].

Doping graphene offers an effective method to tune the properties of the pristine material. Increased levels of doping can lead to the opening of a band gap and an increased number of charge carriers but often at the same time decreases the charge carrier mobility [45,64]. To improve the understanding of the effects of doping in graphene, systematic monitoring by structural and electrical characterization methods while continuously changing the doping level offers a viable route.

4. 1D: Graphene nanoribbons

Another approach to readily tailor the electronic properties of graphene and a very promising route to open up a large band gap is geometrical confinement into nanometer-wide GNRs [22]. Soon after the experimental breakthrough of graphene, GNRs were recognized as materials with great potential for a variety of applications, because of the possibility of precisely tailoring their properties through the variation of their edge geometry and width [69–71]. According to the different edge structures, GNRs can be divided into several classes, including armchair GNRs, zigzag GNRs, chevron-type GNRs, and cove-edge GNRs [20,72,73]. Among all these different structures, armchair GNRs have attracted tremendous research interest because of their high chemical stability, and large and tunable band gap energy. Interestingly, the electronic structure of armchair GNRs (N-AGNRs, where N is the number of carbon atoms across the ribbon) has been shown to be extremely sensitive to the ribbon width, and can be divided into three

subfamilies with $N_1 = 3p$, $N_2 = 3p + 1$, and $N_3 = 3p + 2$ $(p = 1, 2, 3, \ldots)$ [22,74]. For a comparable width, the predicted band gaps decrease drastically from N_2 to N_3 while N_1 typically shows intermediate values. Moreover, the width of the ribbons in the three subfamilies has been predicted to play an important role in tuning the polarity of carrier transport in AGNRs. Therefore, it is of primary interest to engineer and investigate the electronic structures and transport properties of AGNRs by tuning their width and edge structures. “Bottom-up” synthesis has indeed enabled the fabrication of ultra-narrow ($\sim 1 - 2$ nm) GNRs and demonstrated large band gaps of $\geq 1 - 2$ eV as well as visible to near-infrared absorption [27,75–81] rendering them highly interesting materials for a broad range of applications in next-generation transistors, as well as optoelectronic and photonic devices [82–84].

4.1. Synthesis of GNRs on catalytic surfaces

The fabrication of GNRs was first reported by top-down approaches, such as lithographical patterning of graphene [85,86], ultrasonication breaking of graphene sheets [87], and unzipping of carbon nanotubes [88,89]. However, most of the GNRs obtained are wider than 10 nm and exhibit limited gate modulation [85,86]. Besides, the width and edge structures of these top-down fabricated GNRs are poorly controlled. To remedy this, the bottom-up approaches have been developed to synthesize atomically precise GNRs. The tailor-made molecular precursors are chosen as building blocks for synthesis of the structurally well-defined GNRs by surface-assisted [20,90,91] or solution-mediated [27,76–79] polymerization into linear polyphenylenes followed by oxidative cyclodehydrogenation or “graphitization”. With the capability of tailoring the monomer building blocks by modern synthetic chemistry [80], the bottom-up approach renders the access to molecular-scale design of GNRs with engineered chemical and electronic structures that cannot be achieved by the top-down approach. In the bottom-up synthesis methods, bulk-scale synthesis of liquid-phase-processable GNRs has been reported. The polymerization is the key step in the solution-mediated synthesis of GNRs, which

determines the final structures of the GNRs as well as their length. For example, we have reported a use of the AB-type Diels-Alder polymerization for the preparation of cove-type GNRs with high longitudinal extension over 600 nm [27,75]. A_2B_2-type and AB-type Suzuki-Miyaura polymerization have been reported for synthesis of armchair GNRs by our group [78] and Dong *et al.* [92], respectively. By using various halogen group substituted monomers, an AA-type Yamamoto polymerization has been used for synthesis of various cove-edge [73] and chevron-type GNRs [79,93]. While most of the reported GNR synthesis solely relies on the cyclodehydrogenation reaction in the graphitization step, Loo *et al.* [94] and Chalifoux *et al.* [95] have reported the synthesis of narrow armchair GNRs using alkyne benzannulation reactions. Despite the remarkable progress of the solution-mediated approach, processing of the solution-synthesized GNRs is still a major obstacle due to their limited solubility and tendency to aggregate in dispersions, compromising the performance of the electronic devices made with them: The I_{on}/I_{off}-ratio of only up to ~5 has been observed despite the large band gap of ~2 eV [96–98]. To solve this problem and make the GNRs suitable for device applications, in collaboration with the group of Roman Fasel our group achieved the bottom-up synthesis of atomically precise GNRs on a metal surface in an ultrahigh vacuum (UHV) condition [20]. In this surface-assisted approach, monomers substituted with halogen groups are coupled into linear polyphenylenes via radical polymerization, which subsequently undergo cyclodehydrogenation into atomically precise GNRs of different topologies and widths. By design and synthesis of various monomers, we have succeeded in the synthesis of GNR structures, including 7-AGNRs [20], chevron-type GNRs [20], 6-ZGNRs [99], and even GNR heterojunctions [90]. Inspired by our work, other groups have also worked on GNR synthesis using this surface-assisted UHV method, and reported other GNRs such as narrow 5-AGNRs [100], wider 13-AGNRs [101], and heteroatom doped GNRs [102–104]. However, the elaborate and costly UHV equipment restricts the large-scale fabrication and further use of the

GNRs. Sakaguchi *et al.* have proposed the use of the CVD method for the on-surface synthesis of GNRs, with a two-zone furnace system under low pressure, and reported the fabrication of three different armchair GNRs [105] and more recently cove-edge GNRs [106].

We have independently developed an efficient CVD process for the inexpensive and high-throughput bottom-up synthesis of structurally defined GNRs and recently reported fabrication of chevron-type GNRs and 7-AGNRs (subfamily $N = 3p + 1$) over large areas even under ambient-pressure conditions (**Figure 4**) [28]. Notably, the CVD-grown GNRs exhibit structural quality and properties comparable with those synthesized under UHV conditions as manifested by Raman, high-resolution electron energy loss spectroscopy (HREELS), X-ray photoelectron spectroscopy (XPS), and scanning tunneling microscopy (STM) analyses. Because of the high versatility, our CVD process provides access to a broad class of GNRs with designed structures and properties, e.g. 9-AGNRs of subfamily $N = 3p$ and 5-AGNRs of subfamily $N = 3p + 2$ by using different monomers **(Figure 5)** [107]. Our "bottom-up" CVD method further allows for the growth of N-doped and N, S-co-doped GNRs using nitrogen and sulfur containing monomers. Moreover, fabricating heterojunctions such as p-N-GNRs with seamlessly connected segments of pristine (p) and N-doped (n) GNRs was also achieved by co-depositing the pristine monomer and its N- substituted equivalent on a Au/mica substrate in a CVD growth [28]. Our CVD synthesis process thus furnishes GNRs with engineered topographic and chemical structures, which ensures the possibility to study the relationship between the structures and electronic properties of different GNRs.

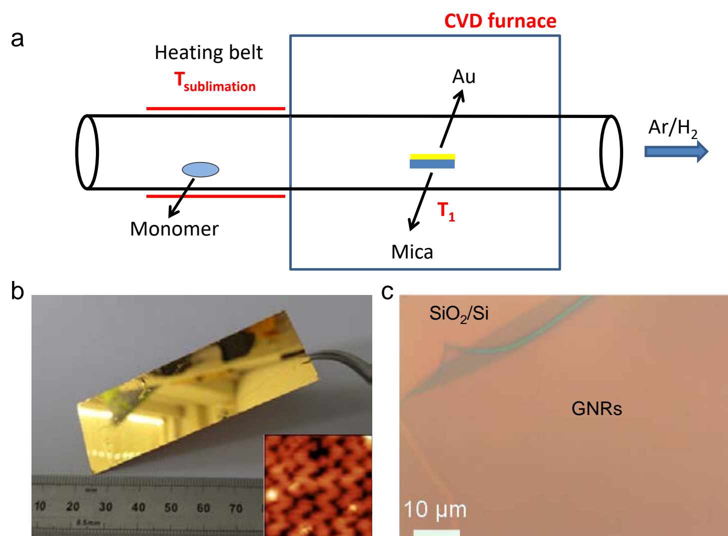

Figure 4: CVD synthesis of GNRs. a) Scheme of a two-zone ambient-pressure CVD system for GNR growth. b) Photograph of a 25×75 mm^2 GNRs/Au/mica plate. Inset shows the STM image of the CVD-grown GNRs. c) Optical microscope image of the GNR film transferred on SiO_2/Si substrate. Reproduced with permission from Ref. [28]. Copyright 2016, American Chemical Society.

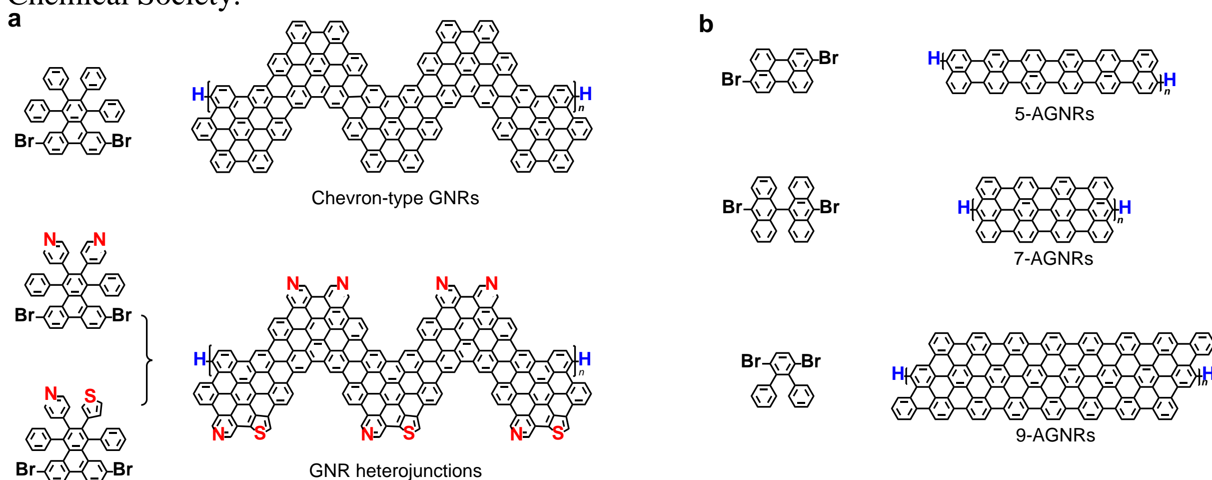

Figure 5: Catalogue of molecular precursors for the CVD synthesis of structurally defined chevron-type GNRs and their heterojunctions (a), and armchair GNRs with different width (b).

4.2. Electronic properties of bottom-up synthesized GNRs

In the course of a continuing miniaturization of electronics, one major vision is the implementation of a single GNR in a working electronic device, such as a single GNR-field effect transistor (single GNR-FET). This goal is nevertheless a tremendous technological challenge with two main steps to take: The first one is the deposition of a single isolated

nanoribbon at a pre-defined location on a chip or wafer-substrate. Secondly, a reliable electrical connection has to be established. Several attempts have been reported on the fabrication of single GNR-FETs, but the device performance has been significantly compromised by the dominant contact resistance (*vide infra*) [28,108]. We have recently investigated, both, short channel devices aiming to probe only one or few ribbons, and long channel devices, demonstrating the charge transport properties of GNR networks [28].

4.2.1. GNR transfer process

A way to avoid the first drawback could be to adapt the synthesis process of the nanoribbons such, that they already grow at a desired location or in an aligned fashion [109,110]. However, in most cases the GNRs are grown either in solution or on a metallic surface as described and have to be deposited on the surface of an insulating substrate in order to fabricate a device based on charge transport. For GNRs grown on metallic surfaces, methods have been developed to transfer the as-grown GNR film as a whole to an insulating substrate such as Si/SiO_2 [20,28,108]. In order to avoid degradation of the GNRs some of these methods have been devised to not involve sacrificial polymer layers such as poly(methyl methacrylate) (PMMA) as described elsewhere [28].

4.2.2. Charge transport in bottom-up synthesized GNRs

Two complications come along with the use of GNRs as a transistor material: Firstly, the typical length of bottom-up synthesized GNRs ranges from tens to hundreds of nanometers, meaning that the active channel length in a transistor becomes very small. In the case of traditional MOSFETs, “small” means that the channel length is comparable to the lateral extent of the depletion layers of source and drain electrode [111,112] and the consequences that arise for its operation are subsumed under the term “short-channel-effects“. There are predictions for graphene and GNRs that the reduced channel thickness (graphene is ultimately thin with only

one atom) makes it more robust against such short-channel effects. However, experimental evidence [113,114] is scarce here, which calls for further studies.

Secondly, to establish Ohmic contacts to a nano-object with a very small surface area and being only one atom thick is yet of greater importance, as the series resistance between channel and electrodes has an even higher impact than the gate length reduction [115,116]. Many reports attempting to fabricate single GNR-FETs discuss the issue of Schottky-like energy barriers at the metal/GNR interfaces, which inhibit the current flow and are thus one major limitation of charge injection in single or few-ribbon devices [28,108,117]. Such barriers due to band mismatch between channel and contact metal degrade the transistor performance and lead to limited I_{on}/I_{off}-ratios. Although a pronounced field effect [28] is regularly observed in long channel devices, the situation is often not as clear in short channel devices. In **Figure 6** we exemplarily show a measurement of a short channel device where the dependence of the channel-current on gate voltage is negligible. A second factor contributing to the masking of the electric field effect is the ratio of channel length and thickness of the gate dielectric. For a thick gate barrier oxide of $t_{SiO2} = 300$ nm the metallic leads will screen a large fraction of the electric field, if the channel length is in the range of only a few nanometers. In a situation where the device resistance is already limited by Schottky-barriers, no field effect can be observed. Alternatively, long channel devices, where the electrode spacing lies in the range of micrometers, offer a certain flexibility for charge transport studies. The fabrication of such devices usually involves fewer steps and less contamination to the GNR channel, since treatment with organic solvents, photoresists and energetic electron beams in lithography processes are minimized or even completely avoided. Such contaminations easily lead to a degradation of the device performance [28,94,96,118,119].

We have thus fabricated devices where the channel lengths of GNR network transistors are approximately 1 - 2 µm (**Figure 7 a, b**). The electrical resistance of the devices can be

modulated by negative gate voltages, indicating a hole-dominated transport. This p-type behavior can be a result of charge transfer doping induced by adatoms and the substrate. For graphene and related materials, it is well established that impurities on a SiO_2 surface [120] as well as atoms and molecules present in ambient conditions such as water [121] act as strong p-dopants. As the measurements in this case have been conducted in ambient conditions and Si/SiO_2 is the supporting substrate, we assume these influences to be present in our samples. A transition of p- to n-type transport has previously been seen by Bennett *et al.* [108]. With an I_{on}/I_{off}-ratio of 6000, such long channel devices show a superior gate modulation of the resistance and they even perform better than ultra-narrow channel devices [108] for devices where SiO_2 is used as a gate barrier. Another proposed use of carbon-based structures is to contact other organic conductors as Schottky barriers that form in contact to metal can be reduced or avoided. Thus, carbon-carbon interactions are beneficial to reduce the contact resistance and to facilitate charge injection. Single and multi-layer graphene has been demonstrated to be an ideal candidate for this purpose [28]. In order to fabricate electronic devices with a reasonable amount of GNRs as an active channel a small separation between two graphene films is needed. It is possible to obtain such a nano-gap by cutting a graphene film into two. On the one hand, electron beam lithography may yield such gaps. However, ultimately small gaps are obtained by employing electromigration, a well-known technique to obtain atomic break-junctions in metals [122]. This method has previously been used to electrically contact ultimately small structures such as single molecular magnets [123]. As we demonstrated, this approach is equivalently suitable to contact GNRs (**Figure 7** a, b). Indeed, we observe an improved contact resistance along with n-type conduction and an I_{on}/I_{off}-ratio of >100 only limited by the gate voltage applied in the measurement. We expect that by further optimizations of growth, transfer and device integration, the exploration of GNRs with their exciting properties will finally become fully accessible. An obvious advantage for this process is that

one can rely on readily existing techniques, developed for reaching the ultimate performance limits of graphene-based devices, e.g. the usage of hexagonal boron nitride as supporting material.

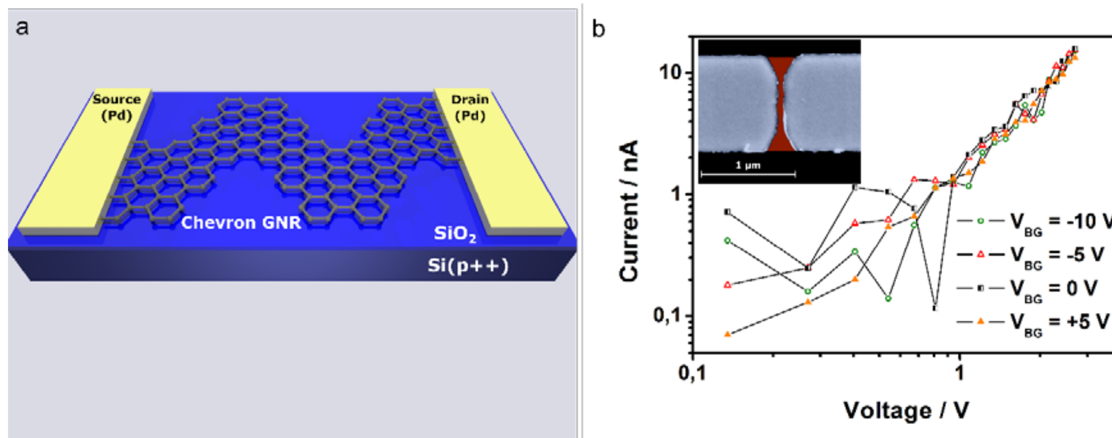

Figure 6: a) Idealized schematic drawing of a single Chevron-GNR field effect transistor. b) I-V-characteristics of a real short channel device. V_{BG} denotes the applied back gate voltage. The inset shows an SEM image of a short channel device, where the Pd-contact electrodes are marked in blue. The area in red is the active GNR-channel. The shortest part of the gap is 45 nm, which is approximately 5 times the average length of a single GNR [28].

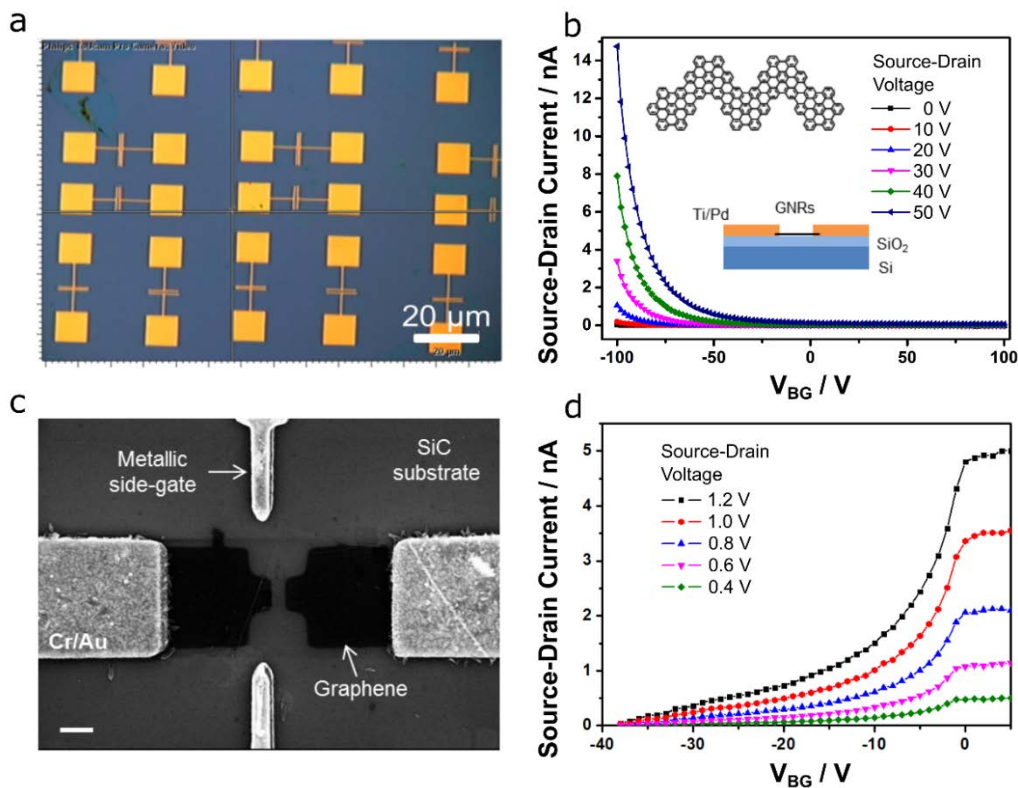

Figure 7: Electrical characteristics of FET devices fabricated with CVD-grown chevron-type GNRs. a) Optical micrograph of long channel device (golden) with a channel length of 1 - 2 µm on a Si/SiO_2-substrate (dark blue background). b) Dependence of source-drain current on back gate voltage measured in the long channel devices. The GNR show a unipolar p-type transport behavior with an I_{on}/I_{off}-ratio of > 1000 in the presented measurement. Inset shows the scheme of the device and the GNR structure. c) SEM image of the device on SiC substrate with graphene contacts. d) Transfer curves of a typical GNR device with graphene electrodes, exhibiting an n-type conduction with high I_{on}/I_{off}-ratio. Adapted with permission from Ref. [28]. Copyright 2016 American Chemical Society.

5. Conclusions

In summary, we have studied three carbon materials with complementary properties, namely TG, doped graphene and bottom-up synthesized GNRs. For TG we have demonstrated 2D-transport properties [13]. The efficient spin injection through transparent contacts renders this material a promising spin conduit in spin-torque devices, where one can efficiently displace magnetic domain walls in a ferromagnetic material.

Hetero-atomic doping in graphene enables a wide range of modifications of its electronic properties e.g. a band gap opening and the modulation of the charge carrier density [45,64]. In CVD-synthesized N-doped graphene, the nitrogen dopants contain mainly three different

bonding configurations (graphitic N, pyridinic N and pyrrolic N) which distribute across the sample depending on the growth conditions. Each configuration changes the electronic structure and thus charge transport properties in a different way [124]. In our work, we find that increasing the level of N-doping leads to a gradual change in the shape of the MR-curve accompanied with a sign change from positive to negative MR. Further studies combining structural and electrical investigation will complete the picture of the electronic structure changing with the configuration and arrangement of the nitrogen dopants in graphene. As an example, we have elucidated that photochemical doping allows one to tune the Fermi level of graphene locally with complex and controllable spatial doping-profiles opening the way for novel applications such as optically defined p-n-junctions [44].

Finally, we have demonstrated the versatility of GNR synthesis by a simple ambient-pressure CVD method, being capable of high-throughput and scalable growth of various GNR structures at low cost for facile device integration. Nevertheless, the device integration of atomically perfect GNRs is still in its early stages. The performances of FET devices fabricated with few or single GNRs are regularly compromised by Schottky-like transport barriers, precluding access to the intrinsic transport properties of the GNRs. We suggest that development of wider GNRs with smaller band gaps and growth of longer GNRs through optimization of the CVD process further reduces the impact of Schottky-barriers and contact resistance. Up to now, the band gaps of the GNRs used for device studies are typically in the range of several eV. Complementary to wider GNRs, development of GNRs in the low-band gap $N = 3p - 1$ family will also facilitate transport experiments on chemically derived GNRs. In parallel, we explore graphitic electrodes where carbon-carbon interactions improve the electrical contact, reducing the contact resistance between electric lead and active channel drastically. Following these routes, GNRs may provide practical solutions to the current challenges for nano-electronic, optoelectronic, and photonic devices in the future.

Acknowledgements

This work was financially supported by the DFG (Priority Program Graphene SPP 1459, KL1811), the Max Planck Society, the ERC (Starting Grant No. ERC-2007-StG 208162 MASPIC and Advanced Grant No. ERC-2010-AdG 267160 NANOGRAPH) the European Science Foundation (ESF) under the EUROCORES Program EuroGRAPHENE within the project GOSPEL (09-EuroGRAPHENE-FP-001), the Seventh Framework Programme within the project Moquas Molecular Quantum Spintronics FET-ICT-2013-10 610449, the Graphene Flagship project No. CNECT-ICT-2013-10 604391 and the European Commission Marie Skłodowska-Curie actions Project No. ITN-GENIUS PITN-GA-2010 264694 as well as the State Research Centre for Innovative and Emerging Materials (CINEMA). N.R. and M.-L. B. gratefully acknowledge the Graduate School of Excellence Materials Science in Mainz (MAINZ) GSC 266. N.R. gratefully acknowledges the Carl Zeiss Stiftung. M.-L. B gratefully acknowledges the HaVo-Stiftung.

Received: ((will be filled in by the editorial staff))
Revised: ((will be filled in by the editorial staff))
Published online: ((will be filled in by the editorial staff))

Keywords: graphene, doped graphene, graphene nanoribbons, turbostratic graphene, charge transport

References

1. P. Avouris, Z. Chen, and V. Perebeinos, *Nat. Nanotech.* **2**, 605 (2007).

2. J. Zhu, D. Yang, Z. Yin, Q. Yan, and H. Zhang, *Small* **10**, 3480 (2014).

3. M.-F. Yu, O. Lourie, M. J. Dyer, K. Moloni, T. F. Kelly, and R. S. Ruoff, *Science* **287**, 637 (2000).

4. B. Marinho, M. Ghislandi, E. Tkalya, C. E. Koning, and G. de With, *Powder Technol.* **221**, 351 (2012).

5. E. Pop, V. Varshney, and A. K. Roy, *MRS Bull.* **37**, 1273 (2012).

6. M. Drögeler, C. Franzen, F. Volmer, T. Pohlmann, L. Banszerus, M. Wolter, K. Watanabe, T. Taniguchi, C. Stampfer, and B. Beschoten, *Nano Lett.* **16**, 3533 (2016).

7. N. Tombros, C. Jozsa, M. Popinciuc, H. T. Jonkman, and B. J. van Wees, *Nature* **448**, 571 (2007).

8. J. C. Slonczewski and P. R. Weiss, *Phys. Rev.* **109**, 272 (1958).

9. J. W. McClure, *Phys. Rev.* **119**, 606 (1960).

10. S. Shallcross, S. Sharma, E. Kandelaki, and O. A. Pankratov, *Phys. Rev. B* **81**, 165105 (2010).

11. D. Weckbecker, S. Shallcross, M. Fleischmann, N. Ray, S. Sharma, and O. Pankratov, *Phys. Rev. B* **93**, 035452 (2016).

12. J. Hass, F. Varchon, J. E. Millán-Otoya, M. Sprinkle, N. Sharma, W. A. de Heer, C. Berger, P. N. First, L. Magaud, and E. H. Conrad, *Phys. Rev. Lett.* **100**, 125504 (2008).

13. N. Richter, Y. R. Hernandez, S. Schweitzer, J.-S. Kim, A. K. Patra, J. Englert, I. Lieberwirth, A. Liscio, V. Palermo, X. Feng, A. Hirsch, K. Müllen, and M. Kläui, *Phys. Rev. Applied* **7**, 024022 (2017).

14. K. S. Novoselov, D. Jiang, F. Schedin, T. J. Booth, V. V. Khotkevich, S. V. Morozov, and A. K. Geim, *Proc. Natl. Acad. Sci. U. S. A.* **102**, 10451 (2005).

15. K. S. Novoselov, A. K. Geim, S. V. Morozov, D. Jiang, Y. Zhang, S. V. Dubonos, I. V. Grigorieva, and A. A. Firsov, *Science* **306**, 666 (2004).

16. X. Li and H. Zhu, *J. Materiomics* **1**, 33 (2015).

17. L. Li, Y. Yu, G. J. Ye, Q. Ge, X. Ou, H. Wu, D. Feng, X. H. Chen, and Y. Zhang, *Nat. Nanotech.* **9**, 372 (2014).

18. M. S. Dresselhaus and G. Dresselhaus, *Adv. Phys.* **30**, 139 (1981).

19. L. Banszerus, M. Schmitz, S. Engels, J. Dauber, M. Oellers, F. Haupt, K. Watanabe, T. Taniguchi, B. Beschoten, and C. Stampfer, *Sci. Adv.* **1**, e1500222 (2015).

20. J. Cai, P. Ruffieux, R. Jaafar, M. Bieri, T. Braun, S. Blankenburg, M. Muoth, A. P. Seitsonen, M. Saleh, X. Feng, K. Müllen, and R. Fasel, *Nature* **466**, 470 (2010).

21. A. Javey, J. Guo, Q. Wang, M. Lundstrom, and H. Dai, *Nature* **424**, 654 (2003).

22. Y.-W. Son, M. L. Cohen, and S. G. Louie, *Phys. Rev. Lett.* **97**, 216803 (2006).

23. E. J. Duplock, M. Scheffler, and P. J. D. Lindan, *Phys. Rev. Lett.* **92**, 225502 (2004).

24. V. I. Artyukhov, E. S. Penev, and B. I. Yakobson, *Nat. Commun.* **5**, 4892 (2014).

25. M. He, H. Jiang, B. Liu, P. V. Fedotov, A. I. Chernov, E. D. Obraztsova, F. Cavalca, J. B. Wagner, T. W. Hansen, I. V. Anoshkin, E. A. Obraztsova, A. V. Belkin, E. Sairanen, A. G. Nasibulin, J. Lehtonen, and E. I. Kauppinen, *Sci. Rep.* **3**, 1460 (2013).

26. I. Ibrahim, T. Gemming, W. M. Weber, T. Mikolajick, Z. Liu, and M. H. Rümmeli, *ACS Nano* **10**, 7248 (2016).

27. A. Narita, X. Feng, Y. Hernandez, S. A. Jensen, M. Bonn, H. Yang, I. A. Verzhbitskiy, C. Casiraghi, M. R. Hansen, A. H. R. Koch, G. Fytas, O. Ivasenko, B. Li, K. S. Mali, T. Balandina, S. Mahesh, S. De Feyter, and K. Müllen, *Nat. Chem.* **6**, 126 (2013).

28. Z. Chen, W. Zhang, C.-A. Palma, A. Lodi Rizzini, B. Liu, A. Abbas, N. Richter, L. Martini, X.-Y. Wang, N. Cavani, H. Lu, N. Mishra, C. Coletti, R. Berger, F. Klappenberger, M. Kläui, A. Candini, M. Affronte, C. Zhou, V. De Renzi, U. del Pennino, J. V. Barth, H. J. Räder, A. Narita, X. Feng, and K. Müllen, *J. Am. Chem. Soc.* **138**, 15488 (2016).

29. G. Schmidt, D. Ferrand, L. W. Molenkamp, A. T. Filip, and B. J. van Wees, *Phys. Rev. B* **62**, R4790 (2000).

30. A. H. Castro Neto, F. Guinea, N. M. R. Peres, K. S. Novoselov, and A. K. Geim, *Rev. Mod. Phys.* **81**, 109 (2009).

31. M. Wojtaszek, I. J. Vera-Marun, E. Whiteway, M. Hilke, and B. J. van Wees, *Phys. Rev. B* **89**, 035417 (2014).

32. S. Schweitzer, *Diploma Thesis*, Universität Konstanz, **2012**.

33. N. Motzko, B. Burkhardt, N. Richter, R. Reeve, P. Laczkowski, W. Savero Torres, L. Vila, J.-P. Attané, and M. Kläui, *Phys. Rev. B* **88**, 214405 (2013).

34. D. Ilgaz, J. Nievendick, L. Heyne, D. Backes, J. Rhensius, T. A. Moore, M. á. Niño, A. Locatelli, T. O. Menteş, A. v. Schmidsfeld, A. v. Bieren, S. Krzyk, L. J. Heyderman, and M. Kläui, *Phys. Rev. Lett.* **105**, 076601 (2010).

35. S. Lynum, J. Hugdahl, K. Hox, R. Hildrum, and M. Nordvik (Kvaerner Technology And Research Ltd.) US 20030091495 A1, **2003**.

36. T. Yamaguchi, R. Moriya, S. Oki, S. Yamada, S. Masubuchi, K. Hamaya, and T. Machida, *Appl. Phys. Express* **9**, 063006 (2016).

37. M. Kläui, C. A. F. Vaz, J. Rothman, J. A. C. Bland, W. Wernsdorfer, G. Faini, and E. Cambril, *Phys. Rev. Lett.* **90**, 097202 (2003).

38. V. Panchal, C. E. Giusca, A. Lartsev, N. A. Martin, N. Cassidy, R. L. Myers-Ward, D. K. Gaskill, and O. Kazakova, *2D Mater.* **3**, 015006 (2016).

39. C. J. Docherty, C.-T. Lin, H. J. Joyce, R. J. Nicholas, L. M. Herz, L.-J. Li, and M. B. Johnston, *Nat. Commun.* **3**, 1228 (2012).

40. M. B. Klarskov, H. F. Dam, D. H. Petersen, T. M. Hansen, A. Löwenborg, T. J. Booth, M. S. Schmidt, R. Lin, P. F. Nielsen, and P. Bøggild, *Nanotechnology* **22**, 445702 (2011).

41. F. Joucken, Y. Tison, P. Le Fèvre, A. Tejeda, A. Taleb-Ibrahimi, E. Conrad, V. Repain, C. Chacon, A. Bellec, Y. Girard, S. Rousset, J. Ghijsen, R. Sporken, H. Amara, F. Ducastelle, and J. Lagoute, *Sci. Rep.* **5**, 14564 (2015).

42. L. D'Arsié, S. Esconjauregui, R. Weatherup, Y. Guo, S. Bhardwaj, A. Centeno, A. Zurutuza, C. Cepek, and J. Robertson, *Appl. Phys. Lett.* **105**, 103103 (2014).

43. J. Meyer, P. R. Kidambi, B. C. Bayer, C. Weijtens, A. Kuhn, A. Centeno, A. Pesquera, A. Zurutuza, J. Robertson, and S. Hofmann, *Sci. Rep.* **4**, 5380 (2014).

44. H. I. Wang, M.-L. Braatz, N. Richter, K.-J. Tielrooij, Z. Mics, H. Lu, N.-E. Weber, K. Müllen, D. Turchinovich, M. Kläui, and M. Bonn, *J. Phys. Chem. C* **121**, 4083 (2017).

45. H. Gao, L. Wang, J. Zhao, F. Ding, and J. Lu, *J. Phys. Chem. C* **115**, 3236 (2011).

46. D. C. Elias, R. R. Nair, T. M. G. Mohiuddin, S. V. Morozov, P. Blake, M. P. Halsall, A. C. Ferrari, D. W. Boukhvalov, M. I. Katsnelson, A. K. Geim, and K. S. Novoselov, *Science* **323**, 610 (2009).

47. B. R. Matis, J. S. Burgess, F. A. Bulat, A. L. Friedman, B. H. Houston, and J. W. Baldwin, *ACS Nano* **6**, 17 (2012).

48. S. Agnoli and M. Favaro, *J. Mater. Chem. A* **4**, 5002 (2016).

49. Y.-B. Tang, L.-C. Yin, Y. Yang, X.-H. Bo, Y.-L. Cao, H.-E. Wang, W.-J. Zhang, I. Bello, S.-T. Lee, H.-M. Cheng, and C.-S. Lee, *ACS Nano* **6**, 1970 (2012).

50. S. H. Park, J. Chae, M.-H. Cho, J. H. Kim, K.-H. Yoo, S. W. Cho, T. G. Kim, and J. W. Kim, *J. Mater. Chem. C* **2**, 933 (2014).

51. Y. Xue, B. Wu, L. Jiang, Y. Guo, L. Huang, J. Chen, J. Tan, D. Geng, B. Luo, W. Hu, G. Yu, and Y. Liu, *J. Am. Chem. Soc.* **134**, 11060 (2012).

52. A. L. Friedman, C. D. Cress, S. W. Schmucker, J. T. Robinson, and O. M. J. van 't Erve, *Phys. Rev. B* **93**, 161409(R) (2016).

53. D. Wei, Y. Liu, Y. Wang, H. Zhang, L. Huang, and G. Yu, *Nano Lett.* **9**, 1752 (2009).

54. A. L. M. Reddy, A. Srivastava, S. R. Gowda, H. Gullapalli, M. Dubey, and P. M. Ajayan, *ACS Nano* **4**, 6337 (2010).

55. L. Ci, L. Song, C. Jin, D. Jariwala, D. Wu, Y. Li, A. Srivastava, Z. F. Wang, K. Storr, L. Balicas, F. Liu, and P. M. Ajayan, *Nat. Mater.* **9**, 430 (2010).

56. H. Wang, Y. Zhou, D. Wu, L. Liao, S. Zhao, H. Peng, and Z. Liu, *Small* **9**, 1316 (2013).

57. J. Zhang, J. Li, Z. Wang, X. Wang, W. Feng, W. Zheng, W. Cao, and P. Hu, *Chem. Mater.* **26**, 2460 (2014).

58. H. Gao, Z. Liu, L. Song, W. Guo, W. Gao, L. Ci, A. Rao, W. Quan, R. Vajtai, and P. M. Ajayan, *Nanotechnology* **23**, 275605 (2012).

59. F. Hassani, H. Tavakol, F. Keshavarzipour, and A. Javaheri, *RSC Adv.* **6**, 27158 (2016).

60. S. Some, J. Kim, K. Lee, A. Kulkarni, Y. Yoon, S. Lee, T. Kim, and H. Lee, *Adv. Mater.* **24**, 5481 (2012).

61. R. Lv, M. C. dos Santos, C. Antonelli, S. Feng, K. Fujisawa, A. Berkdemir, R. Cruz-Silva, A. L. Elías, N. Perea-Lopez, F. López-Urías, H. Terrones, and M. Terrones, *Adv. Mater.* **26**, 7593 (2014).

62. Y. Ito, C. Christodoulou, M. V. Nardi, N. Koch, H. Sachdev, and K. Müllen, *ACS Nano* **8**, 3337 (2014).

63. A. C. Ferrari, J. C. Meyer, V. Scardaci, C. Casiraghi, M. Lazzeri, F. Mauri, S. Piscanec, D. Jiang, K. S. Novoselov, S. Roth, and A. K. Geim, *Phys. Rev. Lett.* **97**, 187401 (2006).

64. M. Rein, N. Richter, K. Parvez, X. Feng, H. Sachdev, M. Kläui, and K. Müllen, *ACS Nano* **9**, 1360 (2015).

65. J. C. Prestigiacomo, A. Nath, M. S. Osofsky, S. C. Hernández, V. D. Wheeler, S. G. Walton, and D. K. Gaskill, *Sci. Rep.* 7, 41713 (2017).

66. G. Bergmann, *Int. J. Mod. Phys. B* **24**, 2015 (2010).

67. J. Han, S. Wang, D. Qian, F. Song, X. Wang, X. Wang, B. Wang, M. Han, and J. Zhou, *J. Appl. Phys.* **114**, 214502 (2013).

68. X. Li, J. Zhuang, Y. Sun, J. Bai, Z. Zafar, Z. Ni, B. Jin, and Z. Shi, *Carbon* **82**, 346 (2015).

69. L. Brey and H. A. Fertig, *Phys. Rev. B* **73**, 235411 (2006).

70. Y.-W. Son, M. L. Cohen, and S. G. Louie, *Nature* **444**, 347 (2006).

71. B. Obradovic, R. Kotlyar, F. Heinz, P. Matagne, T. Rakshit, M. D. Giles, M. A. Stettler, and D. E. Nikonov, *Appl. Phys. Lett.* **88**, 142102 (2006).

72. K. Nakada, M. Fujita, G. Dresselhaus, and M. S. Dresselhaus, *Phys. Rev. B* **54**, 17954 (1996).

73. J. Liu, B.-W. Li, Y.-Z. Tan, A. Giannakopoulos, C. Sanchez-Sanchez, D. Beljonne, P. Ruffieux, R. Fasel, X. Feng, and K. Müllen, *J. Am. Chem. Soc.* **137**, 6097 (2015).

74. L. Yang, C.-H. Park, Y.-W. Son, M. L. Cohen, and S. G. Louie, *Phys. Rev. Lett.* **99**, 186801 (2007).

75. A. Narita, I. A. Verzhbitskiy, W. Frederickx, K. S. Mali, S. A. Jensen, M. R. Hansen, M. Bonn, S. De Feyter, C. Casiraghi, X. Feng, and K. Müllen, *ACS Nano* **8**, 11622 (2014).

76. M. G. Schwab, A. Narita, Y. Hernandez, T. Balandina, K. S. Mali, S. De Feyter, X. Feng, and K. Müllen, *J. Am. Chem. Soc.* **134**, 18169 (2012).

77. L. Dössel, L. Gherghel, X. Feng, and K. Müllen, *Angew. Chem. Int. Ed.* **50**, 2540 (2011).

78. X. Yang, X. Dou, A. Rouhanipour, L. Zhi, H. J. Räder, and K. Müllen, *J. Am. Chem. Soc.* **130**, 4216 (2008).

79. T. H. Vo, M. Shekhirev, D. A. Kunkel, M. D. Morton, E. Berglund, L. Kong, P. M. Wilson, P. A. Dowben, A. Enders, and A. Sinitskii, *Nat. Commun.* **5**, 3189 (2014).

80. L. Chen, Y. Hernandez, X. Feng, and K. Müllen, *Angew. Chem. Int. Ed.* **51**, 7640 (2012).

81. A. Narita, X.-Y. Wang, X. Feng, and K. Müllen, *Chem. Soc. Rev.* **44**, 6616 (2015).

82. S. J. Lee, J.-Y. Kim, H. P. Kim, D. Kim, W. J. da Silva, F. K. Schneider, A. R. bin Mohd Yusoff, and J. Jang, *Chem. Commun.* **51**, 9185 (2015).

83. S. Osella, A. Narita, M. G. Schwab, Y. Hernandez, X. Feng, K. Müllen, and D. Beljonne, *ACS Nano* **6**, 5539 (2012).

84. F. Bonaccorso, Z. Sun, T. Hasan, and A. C. Ferrari, *Nat. Photonics* **4**, 611 (2010).

85. Z. Chen, Y.-M. Lin, M. J. Rooks, and P. Avouris, *Phys. E* **40**, 228 (2007).

86. M. Y. Han, B. Özyilmaz, Y. Zhang, and P. Kim, *Phys. Rev. Lett.* **98**, 206805 (2007).

87. X. Li, X. Wang, L. Zhang, S. Lee, and H. Dai, *Science* **319**, 1229 (2008).

88. L. Jiao, L. Zhang, X. Wang, G. Diankov, and H. Dai, *Nature* **458**, 877 (2009).

89. D. V. Kosynkin, A. L. Higginbotham, A. Sinitskii, J. R. Lomeda, A. Dimiev, B. K. Price, and J. M. Tour, *Nature* **458**, 872 (2009).

90. J. Cai, C. A. Pignedoli, L. Talirz, P. Ruffieux, H. Söde, L. Liang, V. Meunier, R. Berger, R. Li, X. Feng, K. Müllen, and R. Fasel, *Nat. Nanotech.* **9**, 896 (2014).

91. Y.-C. Chen, T. Cao, C. Chen, Z. Pedramrazi, D. Haberer, D. G. de Oteyza, F. R. Fischer, S. G. Louie, and M. F. Crommie, *Nat. Nanotech.* **10**, 156 (2015).

92. G. Li, K.-Y. Yoon, X. Zhong, X. Zhu, and G. Dong, *Chem. - Eur. J.* **22**, 9116 (2016).

93. T. H. Vo, M. Shekhirev, D. A. Kunkel, F. Orange, M. J.-F. Guinel, A. Enders, and A. Sinitskii, *Chem. Commun.* **50**, 4172 (2014).

94. J. Gao, F. J. Uribe-Romo, J. D. Saathoff, H. Arslan, C. R. Crick, S. J. Hein, B. Itin, P. Clancy, W. R. Dichtel, and Y.-L. Loo, *ACS Nano* **10**, 4847 (2016).

95. W. Yang, A. Lucotti, M. Tommasini, and W. A. Chalifoux, *J. Am. Chem. Soc.* **138**, 9137 (2016).

96. A. N. Abbas, G. Liu, A. Narita, M. Orosco, X. Feng, K. Müllen, and C. Zhou, *J. Am. Chem. Soc.* **136**, 7555 (2014).

97. U. Zschieschang, H. Klauk, I. B. Müller, A. J. Strudwick, T. Hintermann, M. G. Schwab, A. Narita, X. Feng, K. Müllen, and R. T. Weitz, *Adv. Electron. Mater.* **1**, 1400010 (2015).

98. P. Fantuzzi, L. Martini, A. Candini, V. Corradini, U. del Pennino, Y. Hu, X. Feng, K. Müllen, A. Narita, and M. Affronte, *Carbon* **104**, 112 (2016).

99. P. Ruffieux, S. Wang, B. Yang, C. Sánchez-Sánchez, J. Liu, T. Dienel, L. Talirz, P. Shinde, C. A. Pignedoli, D. Passerone, T. Dumslaff, X. Feng, K. Müllen, and R. Fasel, *Nature* **531**, 489 (2016).

100. A. Kimouche, M. M. Ervasti, R. Drost, S. Halonen, A. Harju, P. M. Joensuu, J. Sainio, and P. Liljeroth, *Nat. Commun.* **6**, 10177 (2015).

101. Y.-C. Chen, D. G. de Oteyza, Z. Pedramrazi, C. Chen, F. R. Fischer, and M. F. Crommie, *ACS Nano* **7**, 6123 (2013).

102. R. R. Cloke, T. Marangoni, G. D. Nguyen, T. Joshi, D. J. Rizzo, C. Bronner, T. Cao, S. G. Louie, M. F. Crommie, and F. R. Fischer, *J. Am. Chem. Soc.* **137**, 8872 (2015).

103. S. Kawai, S. Saito, S. Osumi, S. Yamaguchi, A. S. Foster, P. Spijker, and E. Meyer, *Nat. Commun.* **6**, 8098 (2015).

104. G. D. Nguyen, F. M. Toma, T. Cao, Z. Pedramrazi, C. Chen, D. J. Rizzo, T. Joshi, C. Bronner, Y.-C. Chen, M. Favaro, S. G. Louie, F. R. Fischer, and M. F. Crommie, *J. Phys. Chem. C* **120**, 2684 (2016).

105. H. Sakaguchi, Y. Kawagoe, Y. Hirano, T. Iruka, M. Yano, and T. Nakae, *Adv. Mater.* **26**, 4134 (2014).

106. H. Sakaguchi, S. Song, T. Kojima, and T. Nakae, *Nat. Chem. online publication* DOI:10.1038/nchem.2614 (2016).

107. Z. Chen, H. I. Wang, J. Teyssandier, K. S. Mali, T. Dumslaff, I. Ivanov, W. Zhang, P. Ruffieux, R. Fasel, H. J. Räder, D. Turchinovich, S. De Feyter, X. Feng, M. Kläui, A. Narita, M. Bonn, and K. Müllen, J. Am. Chem. Soc. **139**, 3635 (2017).

108. P. B. Bennett, Z. Pedramrazi, A. Madani, Y.-C. Chen, D. G. de Oteyza, C. Chen, F. R. Fischer, M. F. Crommie, and J. Bokor, *Appl. Phys. Lett.* **103**, 253114 (2013).

109. R. M. Jacobberger, B. Kiraly, M. Fortin-Deschenes, P. L. Levesque, K. M. McElhinny, G. J. Brady, R. Rojas Delgado, S. Singha Roy, A. Mannix, M. G. Lagally, P. G. Evans, P. Desjardins, R. Martel, M. C. Hersam, N. P. Guisinger, and M. S. Arnold, *Nat. Commun.* **6**, 8006 (2015).

110. B. Kiraly, A. J. Mannix, R. M. Jacobberger, B. L. Fisher, M. S. Arnold, M. C. Hersam, and N. P. Guisinger, *Appl. Phys. Lett.* **108**, 213101 (2016).

111. J. J. Liou, F. Schwierz, and H. Wong, *Nanometer CMOS* (Pan Stanford Publishing, Singapore, 2010).

112. Y. Taur and T. H. Ning, *Fundamentals of Modern VLSI Devices: Second Edition* (Cambridge University Press, Cambridge, UK, 2013).

113. H. Sarvari, A. H. Ghayour, Z. Chen, and R. Ghayour, *J. Mater.* **2016**, 1 (2016).

114. M. J. Hollander, H. Madan, N. Shukla, D. A. Snyder, J. A. Robinson, and S. Datta, *Appl. Phys. Express* **7**, 055103 (2014).

115. F. Schwierz, *Nat. Nanotech.* **5**, 487 (2010).

116. S. E. Thompson, R. S. Chau, T. Ghani, K. Mistry, S. Tyagi, and M. T. Bohr, *IEEE Trans. Semicond. Manuf.* **18**, 26 (2005).

117. J. P. Llinas, A. Fairbrother, G. Barin, P. Ruffieux, W. Shi, K. Lee, B. Y. Choi, R. Braganza, N. Kau, W. Choi, C. Chen, Z. Pedramrazi, T. Dumslaff, A. Narita, X. Feng, K. Müllen, F. Fischer, A. Zettl, M. Crommie, R. Fasel, and J. Bokor, ArXiv160506730 (2016).

118. J. Baringhaus, M. Ruan, F. Edler, A. Tejeda, M. Sicot, A. Taleb-Ibrahimi, A.-P. Li, Z. Jiang, E. H. Conrad, C. Berger, C. Tegenkamp, and W. A. de Heer, *Nature* **506**, 349 (2014).

119. W. S. Hwang, P. Zhao, K. Tahy, L. O. Nyakiti, V. D. Wheeler, R. L. Myers-Ward, C. R. Eddy, D. K. Gaskill, J. A. Robinson, W. Haensch, H. Xing, A. Seabaugh, and D. Jena, *APL Mater.* **3**, 011101 (2015).

120. R. A. Nistor, M. A. Kuroda, A. A. Maarouf, and G. J. Martyna, *Phys. Rev. B* **86**, 041409(R) (2012).

121. C. Melios, A. Centeno, A. Zurutuza, V. Panchal, C. E. Giusca, S. Spencer, S. R. P. Silva, and O. Kazakova, *Carbon* **103**, 273 (2016).

122. A. Candini, N. Richter, D. Convertino, C. Coletti, F. Balestro, W. Wernsdorfer, M. Kläui, and M. Affronte, *Beilstein J. Nanotechnol.* **6**, 711 (2015).

123. A. Candini, S. Klyatskaya, M. Ruben, W. Wernsdorfer, and M. Affronte, *Nano Lett.* **11**, 2634 (2011).

124. T. Schiros, D. Nordlund, L. Pálová, D. Prezzi, L. Zhao, K. S. Kim, U. Wurstbauer, C. Gutiérrez, D. Delongchamp, C. Jaye, D. Fischer, H. Ogasawara, L. G. M. Pettersson, D. R. Reichman, P. Kim, M. S. Hybertsen, and A. N. Pasupathy, *Nano Lett.* **12**, 4025 (2012).